Relaxation of a supercritical fluid after a heat pulse in the absence of gravity effects: Theory and experiments

Y. Garrabos
Institut de Chimie de la Matière Condensée de Bordeaux, Centre National de la Recherche Scientifique, Université Bordeaux I, Avenue du Dr. Schweitzer, F-33608 Pessac Cedex, France

M. Bonetti, D. Beysens,* F. Perrot, and T. Fröhlich
Service de Physique de l'Etat Condensé, Commissariat à l'Energie Atomique, Centre d'Etudes de Saclay, F-91191 Gif-Sur-Yvette Cedex, France

P. Carlès
Laboratoire de Modélisation en Mécanique, Centre National de la Recherche Scientifique, Université Paris VI, F-75252 Paris Cedex 05, France

B. Zappoli
Centre National d'Etudes Spatiales, 18 avenue Edouard Belin, F-31055 Toulouse Cedex, France
(Received 9 July 1996; revised manuscript received 23 December 1997)

We study the response of a fluid in near-critical conditions to a heat pulse, in the absence of gravity effects. The fluid under investigation is CO_2 at critical density. It is enclosed in a thermostated sample cell. We apply a theory that accounts for hydrodynamics and a real equation of state. Comparison with experiments performed under reduced gravity on board the MIR orbital station show quantitative agreement and demonstrate that the dynamics of relaxation is ruled by two typical times, a diffusion time t_D and a time t_c associated to adiabatic heat transport, the so-called ''Piston effect'' (PE). Three regions are observed in the fluid. First, a hot boundary layer, developing at the heat source, which shows large coupled density-temperature inhomogeneities. This part relaxes by a diffusive process, whose density and temperature relaxations are slowed down close to the critical point. Second, the bulk fluid, which remains uniform in temperature and density and whose dynamics is accelerated near the critical point and governed by the PE time. At the thermostated walls a slightly cooler boundary layer forms that cools the bulk also by a PE mechanism. The final equilibration in temperature and density of the fluid is governed by the diffusion time t_D, which corresponds to the slowest mechanism. Comparison with a one-dimensional model for temperature relaxation is performed showing good agreement with experimental temperature measurements. A brief comparison is given with the situation in the presence of gravity. [S1063-651X(98)11704-X]

PACS number(s): 05.70.Jk, 44.10.+i, 66.10.Cb, 64.60.Fr

I. INTRODUCTION

Fluids are supercritical when their temperature and pressure are above the critical point temperature and pressure. They exhibit a number of interesting properties (large density, low viscosity, large mass diffusivity), which make them intermediate between liquids and gases. In addition, their isothermal compressibility $[\kappa_T=(1/\rho)(\partial\rho/\partial p)_T]$ becomes very large and their thermal diffusivity $[D_T=\lambda/(\rho Cp)]$ goes to zero when they approach the critical point.

The use of supercritical fluids under conditions of reduced gravity, e.g., for the storage of cryogenic propellants, has raised a number of fundamental questions concerning heat and mass transport phenomena when gravity-driven convections are suppressed. We address in the following the situation where a source of heat is located in the fluid [1,2]. This arrangement minimizes the time constant and is a current means used for pressurizing fluid reservoirs. We analyze experiments performed earlier under reduced gravity on board the MIR station [3,4] in the light of recent theoretical approaches [5–13].

A. Heat transport by the piston effect

The transport of heat in dense pure fluids classically involves the mechanisms of convection, diffusion, and radiation. Recently [1,2,5–23], the understanding of thermal equilibration of a pure fluid near its gas-liquid critical point (CP) has evidenced a fourth mechanism, the so-called ''piston effect'' (PE). This effect originates from the high compressibility of the critical fluid.

A numerical simulation of the Navier-Stokes equations for a one-dimensional (1D) van der Waals gas [13] reveals the basic physical mechanisms giving rise to the PE. When homogeneous bulk fluid enclosed in a two-wall sample cell is suddenly heated from one wall, a diffusive thermal boundary fluid layer (thickness δ) is formed at the wall-fluid interface. Here we consider a fluid sample of unit area and unit mass where L is the characteristic fluid dimension (distance

*Present address: Département de Recherche Fondamentale sur la Matière Condensée, CEA-Grenoble, F-38054 Grenoble Cedex 09, France.

TABLE I. Thermal parameters for CO_2 calculated at various experimental temperatures. The temperature dependence of the pressure along the critical isochore is considered linear (see column 2).

$T_i - T_c$[a] (K)	$(\partial p/\partial T)_\rho$ (MPa K^{-1})	$(\partial p/\partial \rho)_T$ (N m kg^{-1})	Cv (J kg^{-1} K^{-1})	γ_0	D_T (m^2 s^{-1})	t_D[b] (s)	t_0[b] (s)	t_c[b] (s)
16.8	0.17	7340.9	1081	6.6	1.83×10^{-8}	123	3.92	3.4
15.9		6882.4	1090	6.9	1.75×10^{-8}	129	3.71	3.3
0.8		194.2	1740	120.7	1.62×10^{-9}	1389	0.097	0.095
0.6		136.9	1812	164.7	1.33×10^{-9}	1692	0.0631	0.0627
0.4		83.6	1923	252.3	9.95×10^{-10}	2261	0.0358	0.0357
0.2		36.0	2140	525.5	5.93×10^{-10}	3794	0.0138	0.0138

[a]CO_2 critical parameters: $T_c = 304.13$ K, $p_c = 7.376$ MPa, $\rho_c = 467.8$ kg m^{-3}.
[b]Characteristic times calculated using the value $L = 1.5$ mm as estimated from Eq. (14).

between the two walls). Due to the high compressibility of the bulk, the fluid layer expands and acts as a piston, generating an acoustic wave that propagates in the bulk and that is reflected on the second wall enclosing the fluid. Thermal conversion of this pressure wave is, in turn, able to heat the fluid in an adiabatic way. As a result, a spatially uniform heating of the bulk fluid is detected after a few acoustic times $t_a = L/c$ (c is the sound velocity in the fluid). During repeated travels of the pressure wave within the fluid, the bulk temperature progressively grows to reach thermal equilibrium. An additional result inferred from a recent asymptotic analysis of the PE [13] shows that the fluid velocity produced by the expansion of the hot boundary layer reaches its maximum value at the edge of the layer. This value is proportional to the heat power (per unit surface) sent at the wall. The true PE driving force is this velocity that induces the compression of the bulk fluid by a small transfer of matter. The boundary layer thus acts as a converter that transforms its thermal energy into kinetic energy by adiabatic fluid motion. The effect of an energy source, as provided by continuous heating in the fluid, is then markedly different from that of a temperature step at the sample wall, where the heat power decreases with time as the fluid equilibrates.

As initially discussed by Onuki and Ferrell [6,9], the first characteristic time scale for the PE is the time scale (t_0) to transfer from the boundary layer an energy amount [$E_b(t \approx 0)$ in J m^{-2}] able to adiabatically heat the remaining (bulk) fluid (size $L - \delta \approx L$) at the temperature level $\Delta T_b(t \approx 0) \approx [E_b(t \approx 0)/L]/C_v$. C_v (in J m^{-3} K^{-1}) is the specific heat at constant volume. Due to propagating pressure waves within the cell when the PE is active, the energy transfer occurs on an acoustic time scale, i.e. practically instantaneously ($t \approx 0$) when compared to t_0. Temperature equilibration is obtained when the boundary layer temperature $[E_{\mathrm{BL}}(t)/\delta]/C_p$ (with C_p the specific heat at constant pressure in J m^{-3} K^{-1}) reaches $\Delta T_b(t \approx 0)$, i.e., when the time-dependent energy $E_{\mathrm{BL}}(t)$, which has diffused into the boundary layer during t_0, has reached $E_b(t \approx 0)$. One then infers $[E_b(t \approx 0)/\delta]/C_p \approx [E_b(t \approx 0)/L]/C_v$ and $\delta \approx L/\gamma_0$, with $\gamma_0 = C_p/C_v$. A more refined treatment [9,11] gives $\delta = L/(\gamma_0 - 1)$. The value of t_0 can readily be written as $t_0 = \delta^2/D_T$, where D_T is the thermal diffusivity of the fluid.

The second and longer characteristic time scale is the diffusion time t_D on the length scale L, that is,

$$t_D = L^2/D_T. \tag{1}$$

t_D and t_0 are then related through

$$t_0 = \frac{t_D}{(\gamma_0 - 1)^2}. \tag{2}$$

A striking result is the critical speeding up of the PE when going closer to the CP [1,17–19]. As a matter of fact, near T_c, γ_0 diverges and both δ and t_0 go to zero although t_D goes to infinity. This result represents an enormous reduction in the time required by the supercritical fluid to come close to the temperature equilibrium (see Table I). The fluid inhomogeneities, however, continue to relax diffusively [2,13,16], which makes final equilibration determined by the diffusion time scale.

B. Experimental limitations

Although the isothermal compressibility of a perfect gas can also be very large, adiabatic fluid motion can never thermalize such a gas faster than heat diffusion [5,23]. On the contrary, near the CP, adiabatic fluid motion can become more efficient than diffusion and give birth to the mechanism of the PE. That is why nearly all the experiments have been performed very close to the CP, in most cases within a few mK [1,16,18–20,22]. In addition to the difficulties of comparing a one-dimensional (1D) model to real experiments, most of the studies suffer from complications, listed below, that can make the results difficult to analyze.

(i) The PE is difficult to study on Earth. Fluids in the vicinity of the CP are extremely unstable to even minute temperature gradients as a consequence of the Rayleigh and Grashof numbers, which become extremely large near the CP [24]. Gravity-driven convections destroy the thermal boundary layer around the heating point and induce mass flow to the upper cell wall. The relative contribution of the different processes involved is very difficult to estimate [16–18]. To be unambiguous, the determination of the PE dynamics should then be carried out under reduced gravity.

(ii) When experiments are performed under reduced gravity, they reveal other problems. One is the cell homogenization very near the CP, which is difficult to attain during the available experimental times [16,17]. In effect, the inhomogeneities in density, as those resulting from the PE itself, relax diffusively [1,2,13,16,17].

(iii) The dynamics of the PE is sometimes difficult to analyze because the temperature and heat flux at the cell

walls are not well defined [17]. An ideal temperature step is quite difficult to fulfill when considering the large values of equilibration times in the materials classically used (1–10 s) [16,17] compared to the characteristic times of the phenomenon.

As a result, most of the reported observations remain qualitative in nature [14–16,22,25]. In order to circumvent the above problems, we have carried out experiments under weightlessness (using the ALICE instrument on board the MIR Station [3,4]); we have introduced a heat source by using a small thermistor directly immersed in the fluid. Second, we have studied the PE at temperature not very close to the CP in order to adjust the characteristic time scales to the experimental constraints.

Previously [1,2] we have analyzed the fluid evolution under continuous heating by a thermistor. Liquid, gas, and critical densities have been investigated. They all follow the same scaled, universal behavior. A hot boundary layer (HBL) develops diffusively with a thickness that scales as δ and t_0 but grows as $(\text{time})^{2/3}$. This deviation from a classical diffusive expansion in $\sqrt{t}$ corresponds to a transient regime due to the finite size of the heat source [26,27]. Associated to the development of the HBL, the remaining fluid (bulk) undergoes a simultaneous uniform density and temperature increase due to the PE.

In the present paper we investigate the temperature and density relaxation after a 480 ms heat pulse as provided by a thermistor. Our main results are in agreement with the above vision of a HBL, which diffuses and acts as a piston to uniformly heat the remaining bulk fluid. At the same time, since the cell walls are kept at a constant temperature, a complementary cold boundary layer (CBL) develops at the cell-fluid border and uniformly cools the fluid to restore progressively the initial temperature. Diffusion remains the only mechanism by which density inhomogeneities can relax and the fluid eventually reaches complete homogenization.

This paper is organized as follows. In Sec. II we discuss a 1D model. Section III is devoted to the experimental setup. Section IV reports the main observation on Earth and deals with the analysis of the microgravity results. Section V is devoted to the comparison of data with the model. Two appendices are added. In Appendix A, we summarize the derivations of the expressions concerning Sec. II presenting the model. Appendix B gives the heat pulse characteristics using the thermistor self-heating mode.

II. THE 1D MODEL

The 1D model as developed in [13] for a van der Waals gas is extended here to a real equation of state. This adaptation is summarized in Appendix A. Detailed calculations can be found in the referenced paper.

The space variable is x with L being the fluid thickness. The sample is initially at equilibrium temperature T_i and pressure p_i on the critical isochore (density $\rho=\rho_c$) in the vicinity of the CP ($T_i \geqslant T_c$). At time $t=0$, a heat flux $P(t)$ is sent from the cell wall at $x=0$ during the total heating period Δt_H. The temperature regulation of the cell wall at $x=L$ corresponds to the condition $T(x=L,t)=T_i$. The fluid is described by a linearized equation of state and its behavior obeys the 1D compressible unsteady Navier-Stokes equations for Newtonian fluids. The system of equations is solved analytically by a method of singular perturbations (the method of matched asymptotic expansions).

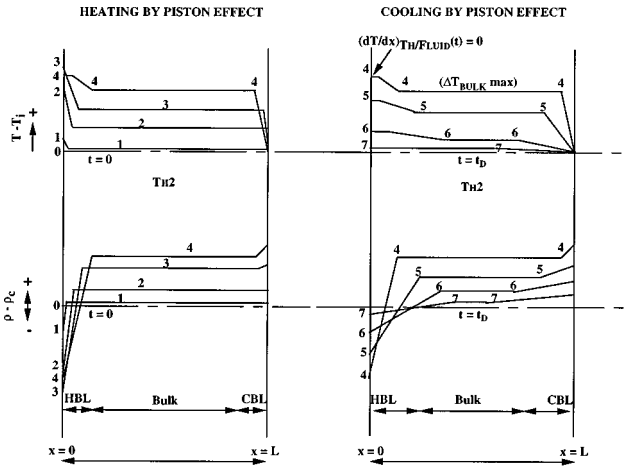

FIG. 1. Schematic behavior of the density $(\rho-\rho_c)$ and temperature $(T-T_i)$ relaxation in a 1D cell model after a heat pulse performed at the $x=0$ wall. Time is referenced to the beginning of the pulse (curves labeled 0). Heat pulse duration (Δt_H) corresponds to the time where the heat flux at the wall differs from zero and, at $t=\Delta t_H$, ΔT_{bulk} reaches a maximum.

As heat is sent into the fluid, a hot boundary layer (HBL) develops at the $x=0$ wall where the fluid expands because of its large compressibility. Here density becomes $\rho<\rho_c$. This expansion induces a compression of the bulk, which in turn causes temperature and density to rise. At the same time a cold boundary layer (CBL) diffuses from the $x=L$ wall, where the fluid contracts, i.e., density becomes $\rho>\rho_c$. The contraction causes an expansion of the bulk and reduces the bulk temperature. The behavior of the fluid is the result of these two competing processes, heating by HBL and cooling by CBL. The typical sequences are schematized on Fig. 1, where the notation is defined. In particular, we denote as *bulk* the fluid region, which does not include the *boundary layers*. It is clear that the spatiotemporal variations of the physical parameters (temperature and density) must be observed over the whole sample for a complete understanding of the PE.

There is no limitation regarding the heat pulse duration (Δt_H) with respect to the PE characteristic time. There is only one limitation in the model: Δt_H has to be short compared to the longest time scale, the diffusive time. Because the diffusive time goes to infinity at T_c while the PE time goes to zero, it is then always possible to analyze correctly the PE dynamics, e.g., by choosing the proper temperature distance from T_c.

A. Thermalization by a heat pulse

In [13], we have considered the response of a fluid after heating and cooling. Various pulse profiles $P(t)$ are applied at the wall at $x=0$. The temperature response in the bulk (T_b) is found under the form of a convolution product $(\otimes)$ of $P(t)$ by a function $F(t)$,

$$T_b(t)-T_i=\left(\frac{P(t)}{mc_v}\right)\otimes F(t), \tag{3}$$

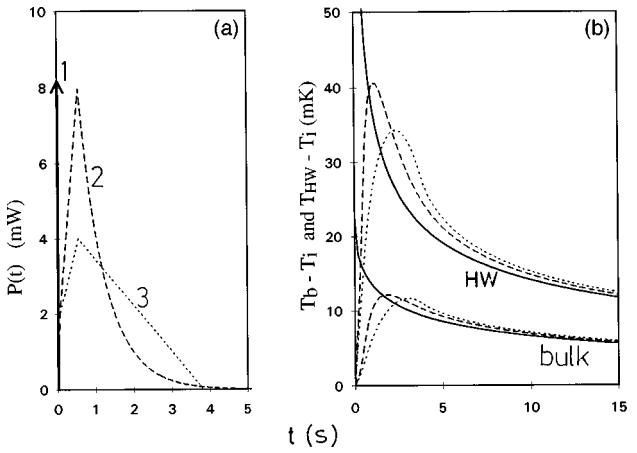

FIG. 2. (a) Three schematic power profiles for heat pulses of the same total energy (8.1 mJ) sent at the boundary $x=0.1$: Dirac function (instantaneous heat pulse corresponding to the Ferrell and Hao model); 2 and 3: finite duration heat pulses; pulse 3 corresponds to the model of the true experimental heat pulse obtained from the 480 ms electrical excitation of the TH1 thermistor (see text and Appendix B). (b) Temperature variations of the bulk, T_b-T_i, (lower curves) and of the hot wall, $T_{\mathrm{HW}}-T_i$ (upper curves) vs time. solid lines: pulse 1; dashed lines; pulse 2; dotted lines: pulse 3.

where m is the total mass of the fluid. In Eq. (3), the function $F(t)$ is

$$F(t)=\exp\left(\frac{t}{t_c}\right)\mathrm{erfc}\left(\frac{t}{t_c}\right)^{1/2}. \tag{4}$$

where the PE dynamics appears to be ruled by the characteristic time t_c:

$$t_c=t_0(1-1/\gamma_0). \tag{5}$$

In Eq. (3), the convolution product reflects precisely the fact that Δt_H can be of order t_c as mentioned above. Then the function $F(t)$ can be considered as the impulse response of the PE. Since γ_0 goes to infinity at T_c, t_c differs from t_0 only far from T_c (see Sec. 2.4).

An interesting feature of Eq. (3) is the fact that at values of t much larger than Δt_H, T_b-T_i tends to behave like $F(t)$ regardless of the time history of $P(t)$. This is illustrated in Fig. 2, where T_b-T_i is calculated for three different heat fluxes $P(t)$ of same total energy Q, the energy effectively transmitted to the fluid at the end of the heat pulse $t=\Delta t_H$ (the numerical values are justified below, Secs. II C and II D). The curves representing the bulk temperature modifications tend to merge after 10 s. This property will be of great help when we try to adapt the model to the experimental pulse (see Sec. V).

In the same way that we found the impulse response of the bulk temperature, it is possible to find the impulse response of any thermodynamic parameters of the system, at all locations x. For instance, the temperature at the hot wall $T_{\mathrm{HW}}(x=0,t)$ can be expressed as

$$T_{\mathrm{HW}}=T_b(t)+\left(\frac{P(t)}{L\rho_c c_p S_{\mathrm{HW}}}\right)\otimes H(t), \tag{6}$$

where S_{HW} is the hot wall surface area. The function $H(t)$ is

$$H(t)=\frac{1}{\sqrt{\pi}}\left(\frac{t_D}{t}\right)^{1/2}. \tag{7}$$

The result that time scales with the diffusive time t_D in the function $H(t)$ reflects the diffusive character of the boundary layer. For a similar analysis as above, Fig. 2(b) gives the temperature variations of the hot wall corresponding to the three different heat pulse profiles of the Fig. 2(a). The curves tend to merge after a few seconds.

Another interesting result of this model is concerned with the fluid velocity u_{HBL} reaching its maximum value at the HBL border given by the following equations:

$$u_{\mathrm{HBL}}=\frac{1}{T_c}\left(\frac{\partial T}{\partial p}\right)_\rho\frac{P(t)}{S_{\mathrm{HW}}}\cong\frac{P(t)}{7p_cS_{\mathrm{HW}}}, \tag{8}$$

where we have used the approximation $(\partial T/\partial p)_\rho\cong T_c/7p_c$ (see Table I). This supports the image of a piston since the velocity is proportional to the heat flux per unit surface sent into the fluid. Heating by PE is thus only effective as long as $P(t)$ differs from zero, i.e., only during Δt_H.

Equation (8) is also valid for the CBL. The corresponding velocity u_{CBL} is proportional to the heat flux through the cold wall (CW, surface area S_{CW}). But here cooling by PE remains effective as long as $T_b(t)-T_i$ differs from zero, e.g., during the whole relaxation period, of order t_D.

B. Energy yield and efficiency

Although the bulk temperature behavior is the result of competition between heating and cooling effects, it is possible to calculate the energy balance resulting only from the heating PE, the equations being linearized. This corresponds to considering the cold wall as adiabatic during Δt_H.

At any time during heating, the energy that is sent into the fluid $E(t)$ is split into energy in the HBL and energy $\Delta E(t)$ in the bulk. The ratio $\zeta=\Delta E(t)/E(t)$ is the PE energy efficiency and can be calculated from the model knowing the temperature and density profiles in the cell at all times (see Appendix A). The resulting energy balance between the bulk and the hot boundary layer leads to the following result:

$$\zeta=\frac{\Delta E(t)}{E(t)}\cong\frac{p_i}{T_i}\left(\frac{\partial T}{\partial p}\right)_\rho. \tag{9}$$

The yield ζ is time independent. It varies only slightly with (T_i-T_c). For a van der Waals fluid,

$$\zeta=1/4. \tag{10}$$

For real fluids where $(\partial T/\partial p)_\rho\cong T_c/7p_c$ (see above and Table I),

$$\zeta\sim 1/7. \tag{11}$$

This energy efficiency is low, which means that most of the energy remains stored in the boundary layer.

Simultaneously, the cold boundary layer slowly develops and induces cooling with the same energy efficiency $\zeta=\Delta E'(t)/E'(t)$ (the prime denotes the energies involved in the cooling process). Therefore, the total energy $\Delta E_b(t)$ in

the bulk is then the balance between the energy transferred by PE from the hot wall, $\Delta E(t)$, and the energy lost by PE at the cold wall, $\Delta E'(t)$. The energy effectively transmitted to the bulk $\Delta E_b(t)$ reads as

$$\Delta E_b(t)=\Delta E(t)-\Delta E'(t)=\zeta[E(t)-E'(t)]. \quad (12)$$

The remaining energy is stored in the boundary layers.

Note that, at any time and according to Eq. (3), the first-order bulk temperature is

$$\Delta T_b(t)=\frac{E(t)-E'(t)}{mc_v}, \quad (13)$$

where $E(t)-E'(t)$ is the total amount of energy stored in the fluid at time t. $\Delta T_b(t)$ is precisely the temperature that would have been reached if all this energy had diffused into the bulk. As far as temperature equilibration is concerned, the PE is thus very efficient. This remark seems to be paradoxical with the fact that the energy efficiency is low, with only $\zeta\approx 1/7$ of the total energy sent into the bulk. This can be explained by the fact that the internal energy of a near-critical fluid significantly depends on density; here the bulk density is changed precisely by the small flux of matter at the HBL border [see Eq. (8)].

C. Adaptation of the length scales to a 3D experiment

When $P(t)$ is known, the estimation of the length scale L is critical for a correct adaptation of the 1D model to experiments. The determination of this length is guided by various criteria. There are, however, some ambiguities when considering a real, 3D sample. For instance, L can be the distance between the heat source and the closest wall, or L can be the cell diameter, etc.

A dimensional analogy can be adopted. The heat flux at the cold wall (cooling) depends on the wall area, S_{CW}. For the case of the cooling relaxation which must be the remaining slower mechanism for $t>\Delta t_H$, the correct dimensional analogy between the 1D model and the experiment ensures the same ratio between the volume of fluid to be cooled and the area of the cold wall. We find as a characteristic length

$$L=(\text{cell volume})/(\text{cold wall area})=1.5 \text{ mm}. \quad (14)$$

The numerical value is inferred from the cell dimensions given below (see Sec. III A). In the following we will adopt this value, a choice that will be justified when comparing the model to the experimental data (see Sec. V A 2).

Note that this definition of the characteristic length leads to a slight modification of the model when the HW and CW areas are different as is the case in this experiment. In a linear approximation the amplitudes of local temperature and density in the hot boundary layer have to be magnified by the ratio $S_{\mathrm{CW}}/S_{\mathrm{HW}}\cong 80$ (see Sec. III A). In the 1D model, $S_{\mathrm{CW}}/S_{\mathrm{HW}}=1$. This peculiar result is detailed below in our analysis of the HBL relaxation (see Sec. V B 1).

D. Comparison with the Ferrell and Hao model (Ref. [11])

Ferrell and Hao have considered the cooling of an adiabatic fluid after a Dirac function pulse, $P(t)=Q\delta(t)$. They found for the bulk temperature evolution [9,10],

$$T_b(t)-T_i=\left(\frac{\overline{Q}}{mc_v}\right)F_{\mathrm{HT}}(t), \quad (15)$$

where

$$F_{\mathrm{HT}}(t)=\exp\left(\frac{t}{t_0}\right)\mathrm{erfc}\left(\frac{t}{t_0}\right)^{1/2}. \quad (16)$$

Equation (16) can be compared to Eq. (4) where t_c is replaced by t_0. The Ferrell and Hao model corresponds to the impulse response of our model, when the heat pulse duration is much shorter than the time scale of the PE. We note that the approach in [11] does not give the temperature behavior in the boundary layer since the initial value of this temperature (at $t=0$) should theoretically be infinite for a Dirac heat pulse ($\Delta T_H=0$). In Fig. 2(b) are reported the illustrative results for $T_b(t)-T_i$ calculated using Eqs. (15) and (16) and for $T_b(t)-T_i$ calculated using our Eqs. (3) and (4) when the heat pulse profiles are of finite duration [see the Fig. 2(a) where three schematic profiles are used for the same total energy $Q=8.1$ mJ]. As a consequence of the basic differences enclosed on each of these theoretical approaches, only the long-time behavior ($t\gg\Delta t_H$) of the cooling relaxation collapses on the same single curve.

Both models are linear to first order and become equivalent when the CP is approached. In particular, we obtain the same asymptotic solution for the characteristic time of the PE ($t_c\simeq t_0$ near T_c). Far from T_c, the small difference between the two characteristic times [see Eq. (4)] originates from the slightly different approximation made in the two models.

III. EXPERIMENTAL SETUP

Some aspects of the experimental setup are given in [1]. Since this work deals with the study of various time scales, we report here additional details concerning the geometrical arrangement and the characteristic thermal responses of the different containers. In addition, we try to give the most representative description of the energy sent into the fluid.

A. The cell unit

The experimental cell is filled with CO_2 (air liquide, of purity better than 99.998%) at a critical density of 467.9 kg m^{-3} with an accuracy better than 0.1%. The CuBe cell [Fig. 3(a)] is a parallelepipedic block of external dimensions $17\times 24\times 27$ mm made of copper-beryllium alloy. The fluid is enclosed in a cylinder of 11.6 mm diameter and 6.7 mm thickness (hereafter denoted e) closed at each end by sapphire windows.

The cell is mounted in a sample cell unit (SCU) made of electrolytic copper. The cell is located close to the SCU center of symmetry. The SCU is a cylinder (60 mm external diameter, 115 mm long), which can be cooled and heated by means of Peltier elements located at its top and bottom. The SCU is the central part of a high precision thermostat whose temperature stability is better than 50 μK and temperature gradients are less than 100 μK cm^{-1}. The temperature is controlled and measured by two stabilized thermistors model no. YSI 44900 from Yellow Springs Instrument Co. One

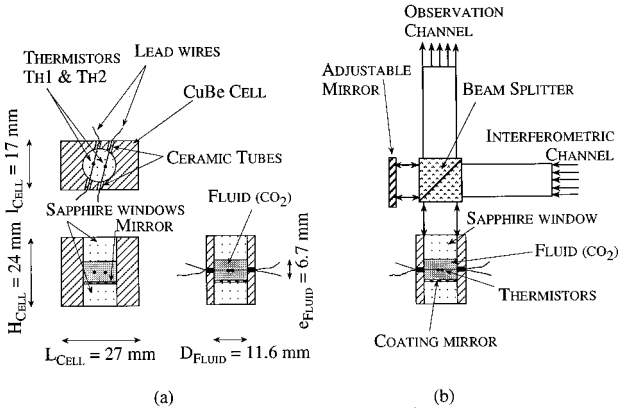

FIG. 3. Experimental setup used for the study of the thermal relaxation in supercritical fluids. (a) Interferometric fluid cell. (b) Twyman-Green interferometer.

thermistor, hereafter called YSI-M, is located close to the fluid cell and is used to determine the cell temperature. The other thermistor is close to the bottom Peltier elements and is used for temperature control.

B. Bulk density measurements

The cell is a part of a Twyman-Green interferometer located in the SCU [Fig. 3(b)]. The interference patterns are detected by a charge-coupled device (CCD) video camera working at 25 frames s^{-1}. The interference pattern provides quantitative measurements of the fluid refractive index and thus of its density. At each equilibrium temperature, the pattern in the sample cell exhibits about 40 parallel straight fringes corresponding to a homogeneous density within the pattern. A reference pattern is given on Fig. 4(a) (for $T_i = T_c + 16.8$ K) and schematized on Fig. 4(b) for practical analysis. The variation δf of the fringe number is related to the fluid thickness e, the refractive index variation δn and the light wavelength ($\lambda = 633$ nm) through

$$\delta f \lambda = 2 e \delta n. \tag{17}$$

Density changes in the fluid result in a local refractive index variation and fringes are shifted and/or distorted. By using the Lorentz-Lorenz relationship

$$\frac{n^2-1}{n^2+2}\frac{1}{\rho} = \text{const}, \tag{18}$$

which connects refractive index n and density, it is possible to infer the relative density variation per fringe shift

$$\frac{\Delta\rho}{\rho} \cong \frac{\lambda}{2(n-1)e}\ \delta f \approx 0.04\% \ \text{ per fringe} \tag{19}$$

[in Eqs. (18) and (19) we have used the critical value $n_c \simeq 1.108$ for the refractive index; the bulk mean density is assumed close to the critical density]. This shift is then counted as the number of fringes that cross a reference line parallel to the initial fringe orientation. The sign (+ or −) of the density variation can be inferred from the direction (left or right) of the pattern's shifting, as will be shown later on Fig. 7 (heating pulse case) and Fig. 11 (continuous heating case [1]). See also the schematic representations of the interferometric images of the cell given on Figs. 4(b) and 4(c).

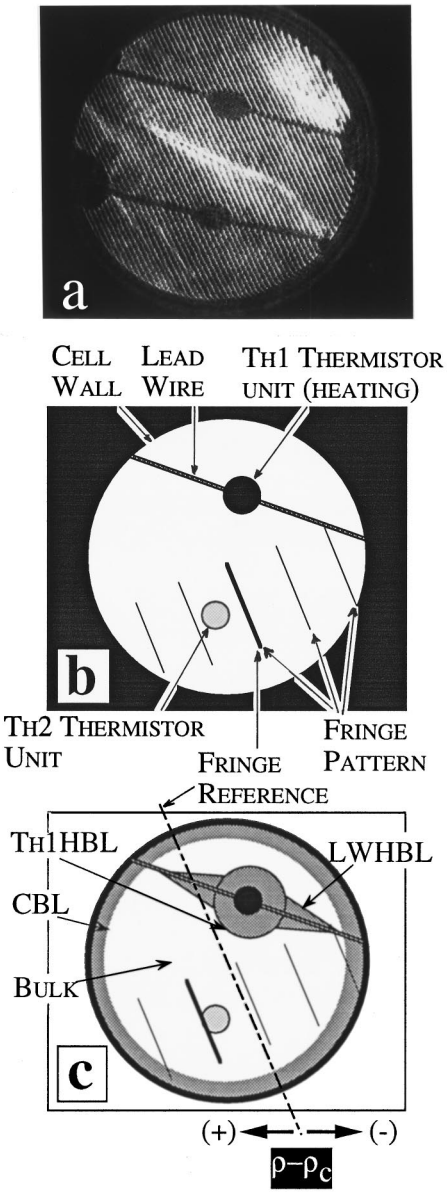

FIG. 4. (a) Interferometric view of the critical sample cell at equilibrium temperature $T_i = T_c + 16.8$ K. The fringes are parallel lines. (b) Schematic presentation of the interferometric view at equilibrium with an arbitrary reference line parallel to the fringes. (c) Same as (b) during the heat pulse performed by the TH1 thermistor (see Figs. 7 and 11); in the selected areas (labeled Bulk, TH1 HBL, LWHBL, and CBL) we observe a shift or distorsion of the fringe pattern. These pattern modifications from the direction of the reference line (left or right) are related to the sign (+ or −, respectively) of the relative density changes from the critical density.

C. Fluid temperature measurements

The thermistors TH1 (the heat source) and TH2 (the bulk temperature measurement) are directly immersed in the fluid at equal distance from the two windows. The separation distance between their centers (4.6 mm) compares well with the thermistor-wall distance (3.5 mm).

TABLE II. Thermal parameters for the various containers involved in the temperature relaxation of the experimental cell. Time constants $t_{R,X}$ are evaluated for the spherical geometry of the X containers except in the lead wires cases (*) (see text).

X part Geometry (material)	Dimensions Volume (m^3)	Φ_{sphere} (m)	Density ($kg\ m^{-3}$)	Effective mass (kg)	C_P ($J\ kg^{-1}\ K^{-1}$)	D_T ($m^2\ s^{-1}$)	$t_{R,X} \cong (\phi/2\pi)^2 D_T^{-1}$ (s)
SCU	$\phi \times H$ (mm^2)						
Cylinder	60×115	72.0×10^{-3}	8950	2.5	385	$1{,}1 \times 10^{-4}$	1.2
(Electrolytic copper)	325×10^{-6}						
Cell	$L \times 1 \times H$ (mm^3)						
Parallelipedic	$27 \times 17 \times 24$	21.8×10^{-3}	8200	74×10^{-3}	419	0.34×10^{-4}	0.35
(Cu-Be alloy)	11×10^{-6}						
Windows	$\phi \times H$ (mm^2)						
Cylinder	$11.6 \times 8.5 (\times 2)$	10.3×10^{-3}	3986	(7.1×10^{-3})	800	0.12×10^{-4}	0.22
(Sapphire)	1.8×10^{-6}						
Thermistors	ϕ (mm)						
Sphere	$0.9 (\times 2)$	0.9×10^{-3}	5200	2×10^{-6}	750	0.26×10^{-6}	0.079
(Zirconia)	0.38×10^{-9}						
Lead wires	$\phi \times H$ (mm^2)	$(\cong 2H)$ (*)					
Cylinder	$0.1 \times 5.25 (\times 2)$	$(11\text{–}16) \times 10^{-3}$	21400	1.8×10^{-6}	134	0.24×10^{-4}	1–2 (*)
(Platinum alloy)	82.5×10^{-12}						

The thermistors are identical (THERMOMETRICS, B35 PB 103 F-A, 100 ms time constant, 35 mW maximum power rating). They are nearly spherical in shape with 0.9 mm diameter. The thermistor is sealed on thin wires of platinum alloy and the whole is encapsulated in a shock resistant glass coating.

Temperature measurements have been performed around $T_c + 16$ K and $T_c + 0.5$ K in a 2-K range, within a resolution of a few mK and a sampling rate of 25 or 0.1 s^{-1}. Temperature data cannot be obtained while TH1 is activated for heating.

Each thermistor in the measurement mode is supplied with a 500 mV regulated voltage; the dissipated power remains generally lower than 4.5 μW, a value obtained when the higher sampling rate acquisition is used in the $T_c + 16$ K temperature range. From the technical data provided by the supplier, the corresponding maximum temperature elevation can be estimated to be around 3 mK. This value has been indirectly confirmed by a careful analysis of the temperature measurements (see Secs. IV D and V B 1), and has therefore been subtracted from the values measured at the maximum sampling rate (the average power is of order of 2×10^{-2} μW at the lower sampling rate; no temperature correction has been needed in this case).

D. Thermal characteristics of the container

A representation of the SCU as an ensemble of spherical containers showing the same volume to surface ratio provides characteristic lengths whose values are listed in Table II (this practical analogy is suggested from the near spherical shape of the internal heating thermistor). The typical thermal response $t_{R,X}$ of a container part labeled X corresponds to the attainment of 63% of the final equilibrium temperature. The $t_{R,X}$ are listed in Table II. Note that these values differ from the 1D diffusive times $t_{D,X}$ by a factor π^{-2}. We shall make the following three remarks.

(i) In order to reduce the thermal time constants of the cell and of the thermostat, the cell body is made of copper beryllium alloy and the windows of sapphire, which leads to $t_{R,\text{cell}} \approx 1$ s. The condition necessary to study the dynamics of cooling ($t_c > t_{R,\text{cell}}$) is fulfilled for $T - T_c > 1$ K (Table I).

(ii) The thermal response of the lead wires (LW) enters into the dynamics of pulse heating. The leads couple the thermistor, where heat is produced, to the SCU, whose temperature is stabilized. The analogy with a spherical problem is not relevant anymore. The length scale reported in Table II corresponds to the distance between the thermistor and the external surface of the cell. The corresponding time constant is $t_{R,\text{LW}} \approx 2$ s.

(iii) The thermal time response of the SCU is comparable to the cell response (Table I). The central location of the cell in the SCU ensures thermal equivalence between the Peltier elements when they react from the heat production in the cell. We note that the temperature of the cell, as measured by YSI-M, exhibits a time constant of 2 s comparable to the SCU thermal time.

From the above analysis, it is possible to infer a characteristic time $t_{\text{YSI}} \cong 2 \pm 1$ s, at which a modification of the fluid temperature can be detected at the YSI-M level.

E. Heat pulse characteristics

When thermistor TH1 is used as a heater, a stabilized voltage of 10 V is delivered during $\Delta t_{\text{elec}} = 480$ ms through a temperature stabilized resistor of 274 Ω in series with the thermistor. The dissipated power is a function of the thermistor resistance, which itself is a function of the local temperature. The power produced inside the thermistor is thus a function of time and of the temperature distance from T_c. The typical range is 5–35 mW depending on the self-heating mode of the thermistor unit.

Since experimental information cannot be obtained on Earth where the thermal exchange is modified by convection

during Δt_{elec} (see below Sec. IV A), we had to develop a model to describe the TH1 behavior. This model is reported in Appendix B where a schematic representation of the energy partition is given in the Fig. 15. It appears that only 50% of the total energy which is produced during Δt_{elec} in the thermistor core is transferred in the HBL around the thermistor. The remaining energy is lost by solid conduction through the lead wires (during the time $t_{R,\text{LW}}$). Then it is more realistic to admit that TH1 can heat the fluid during an effective heat pulse duration $\Delta t_H \approx \Delta t_{\text{elec}} + t_{R,\text{LW}} \approx 2.5$ s. Details of the power evolution during this effective heating period are given in the Appendix B.

IV. RESULTS

A. Heat pulse under Earth's gravity

For the sake of comparison with the microgravity experiments, we analyze in the following the fluid evolution under the influence of Earth's gravity $(1g)$ (see Fig. 5).

When $t < \Delta t_{\text{elec}}$ [Figs. 5(a) and 5(b)], a plume develops within 100 ms after the beginning of the pulse. This value is of the order of the thermistor time constant. The energy produced during that time is as low as 2 mJ. Convection settles in the fluid during the electrical excitation, extends along the lead wires, and prevents any stable thermal boundary layer from forming around the thermistor [Fig. 5(b)].

When $t \geqslant \Delta t_{\text{elec}}$, convection stops [see Fig. 5(c)] and the fluid cell relaxes to equilibrium [see Fig. 5(d)]. The temperature relaxation at TH1 is reported in Fig. 6 at two typical temperature differences from the CP ($T_c + 16.8$ K and $T_c + 0.2$ K). The temperature after the electric pulse at $T_c + 16.8$ K (5 K, extrapolated to 480 ms, see Fig. 6) is approximately 2 times larger than at $T_c + 0.2$ K (2.5 K, extrapolated to 480 ms). It is the same ratio in electric power as calculated from the resistance values $[R_{\text{TH1}}(T_i = T_c + 0.2\text{ K}) \approx 2\, R_{\text{TH1}}(T_i = T_c + 16.8\text{ K})]$. The temperature relaxation is faster as one approaches T_c.

On Earth, the gravitational flow therefore deeply modifies the heat transfers. In addition to the expected PE, the fast relaxation of TH1 is associated with the viscous relaxation of convective flows, which also increase the heat flux between the thermistor and the thermostat to lower the HBL temperature.

In contrast to TH1, the temperature modification in the bulk is too small to be detected by TH2 and in the SCU by YSI-M. The fringe pattern is disturbed only by the plume and recovers equilibrium a few seconds after Δt_{elec}.

B. Interferometric observations under microgravity

The evolution of a typical pattern at $T_c + 16.8$ K and $T_c + 800$ mK under reduced gravity is reported in Fig. 7. These different videoprints correspond to the schematic drawings given in Fig. 8 where selected areas are defined in Fig. 4(c). Time is relative to the beginning of the pulse.

When $t < \Delta t_H$ (heating period), a HBL develops around the thermistor [TH1 HBL area in Fig. 4(c)] whose characteristics are discussed in [1]. We recall the main features of the phenomenon. The layer appears as a black region, nearly spherical in shape, which shows a well-defined border [Figs. 7(a) and 7(a′)]. The fact that the HBL is optically dark is the result of large density gradients associated with large temperature gradients (the pressure is spatially uniform at this time scale). In Fig. 7(a) one notes the progressive extension of the dark region along the leads axis [LWHBL area in Fig. 4(c)], corresponding to heat conduction through the lead wires between TH1 and the SCU.

A striking observation is the simultaneous shift under weightlessness of the whole fringe pattern, with the fringes remaining straight and parallel as indicated in the schematic drawing in Fig. 8. This bulk phenomenon, which coincides

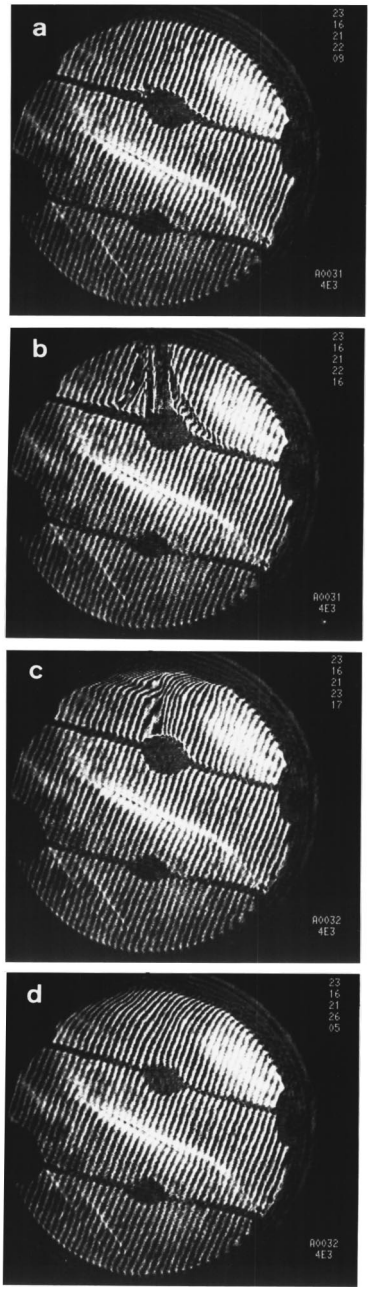

FIG. 5. Heat pulse at the equilibrium temperature $T_i = T_c + 16.8$ K under terrestrial gravity acceleration $(1g)$. Gravity is directed downwards. (a) $t = 80$ ms after the beginning of the pulse, (b) $t = 360$ ms, (c) $t = 1$ s, and (d) $t = 4$ s. Note that the convective plume clearly develops at $t \cong 120$ ms after the beginning of the pulse. At $t = 4$ s, no significant density inhomogeneities could be noticed, which indicates a fast relaxation process.

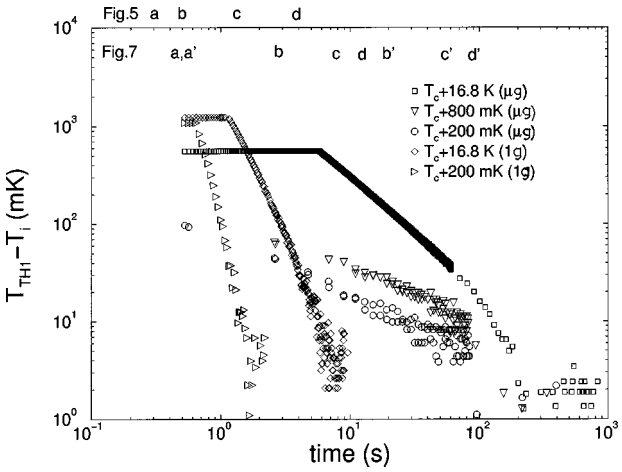

FIG. 6. Temperature relaxation of the heating thermistor TH1 at different equilibrium temperatures after a heat pulse (480 ms electrical excitation) under $1g$ and microgravity conditions. At $T_i = T_c + 16.8$ K, the temperature measurements at short times are limited by the technically available temperature range (see text). Upper part: time reference for the videoprint sequences given on Figs. 5(a)–5(d) ($1g$ conditions at $T_i = T_c + 16.8$ K), in Figs. 7(a)–7(d) (microgravity conditions at $T_i = T_c + 16.8$ K), and in Figs. 7(a′)–7(d′) (microgravity conditions at $T_i = T_c + 800$ mK).

with the growth of the HBL, is the signature of the PE [1]. It corresponds to a spatially uniform density change throughout the entire cell. During the heating period, the pattern shifts to the left, corresponding to a uniform density increase [see Fig. 4(c)]. The process is inverted during the cooling period.

When $t > \Delta t_H$ (cooling period), the HBL continues to develop but at the same time it fades out so that the fringes reappear [see Figs. 7(b)–7(d), 7(b′)–7(d′)]. The bulk pattern slowly returns to equilibrium (parallel fringes). This relaxation mechanism lasts at least 100 s and appears as the largest time scale of the phenomenon. The longer relaxation time for equilibration of the cell at $T_c + 800$ mK with respect to $T_c + 16.8$ K is a consequence of the critical slowing down.

In the following we detail the first few seconds after the end of the electrical excitation.

(i) *The HBL around TH1.* This HBL evolution is similar at all temperatures with a kinetics that slows down when approaching T_c. The layer still expands during the cooling period while simultaneously fading out [Figs. 7(c)–7(d) and 7(c′)–7(d′)].

In order to quantify the extension of the HBL, a simulation of the interferometric fringe pattern as a 2D Gaussian distributed density inhomogeneities within a uniform medium has been made [2] (see Fig. 9). Density inhomogeneities of the order of 1% lower the fringe spacing by a factor of 4 and practically suppress the fringe visibility. We thus define the HBL border as the location of the last distorted fringe. We note the right distortion of the fringes from the direction of the reference line, which reflects the local density decrease within the hot boundary layer [see Figs. 7(c), 7(d), and 8(h)].

We report in Fig. 10 the HBL thickness $\delta_{\mathrm{HBL}} = (\delta - \delta_0)/2$ as a function of time, where δ_0 and δ are the thermistor and HBL diameters, respectively. The HBL diameter is measured at $T_c + 16.8$ K and $T_c + 400$ mK along an axis perpendicular to the lead wire where its perturbative role is minimized. The effective time exponent of the δ_{HBL} growth law can be determined, whose value is close to $\frac{1}{2}$. A numerical simulation as in [1,27] demonstrates scaling by t_D (see Fig. 10).

(ii) *The HBL along the leads.* This HBL along the leads rapidly vanishes in a time nearly independent of T_i [Figs. 8(b)–8(c), 8(b′)–8(c′)]. This phenomenon is due to the heat losses by conduction along the leads. We do not analyze further the corresponding behavior, which can be considered as a complicated perturbative effect.

(iii) *The bulk.* During the cooling period the fringe pattern slowly returns to its initial position, with the fringes remaining straight and parallel. This reverse translation of the pattern shows that the bulk density uniformly comes back to its initial value and demonstrates the existence of a cooling PE. The typical evolution is of order of tens of seconds.

The inversion in the fringe shift occurs after a time of order of 3 s, which corresponds approximately to the heating time Δt_H estimated above. The temperature measurements in the bulk ($T_b = T_{\mathrm{TH2}}$) confirm this interferometric observation (see Sec. IV D).

(iv) *The CBL at the cell wall.* We show in Fig. 11 the formation of a CBL under continuous heating [1]. These figures are clear justification for the schematic representation made in Fig. 4(c). CBL is evidenced by the bending of the fringes at the cell wall while fringes in the bulk remain straight. In contrast to the HBL observation, we note here the left bending of the fringes from the reference line which reflects the increase in density within the CBL. But with our present short pulse, such a layer is difficult to observe as the corresponding density gradient and thickness are very small; moreover, the layer thickness increases while the density gradient decreases with time.

C. Temperature behavior within the HBL

The temperature relaxation of the heating thermistor TH1 is measured at different temperatures from $T_c + 16.8$ K to $T_c + 0.2$ K. We have reported in Fig. 6 a log-log plot of T_{TH1}-T_i as a function of time for three typical temperature differences from T_c ($T_c + 16.8$ K, $T_c + 800$ mK, and $T_c + 200$ mK). When going closer to the CP, the TH1 temperature noticeably decreases (as in the terrestrial observations, although with a different time relaxation).

Two factors are responsible for the lowering of the HBL temperature produced by a constant energy heat pulse: first, the divergence of C_P, which enables the HBL to store more energy; secondly, the critical enhancement of the thermal conductivity λ, which favors the energy transfer from the thermistor into the fluid.

D. Temperature behavior in the bulk fluid

We mainly refer to the bulk temperature evolution at $T_c + 16.8$ K [see Figs. 12(a)–12(c)] as measured by TH2, $T_b = T_{\mathrm{TH2}}$ (corrected at $t < 60$ s by 3 mK due to the thermistor self-heating). Time is counted at the beginning of the heat pulse.

After the electrical pulse has stopped, the temperature still increases. A maximum is reached at about 3 s [see Fig.

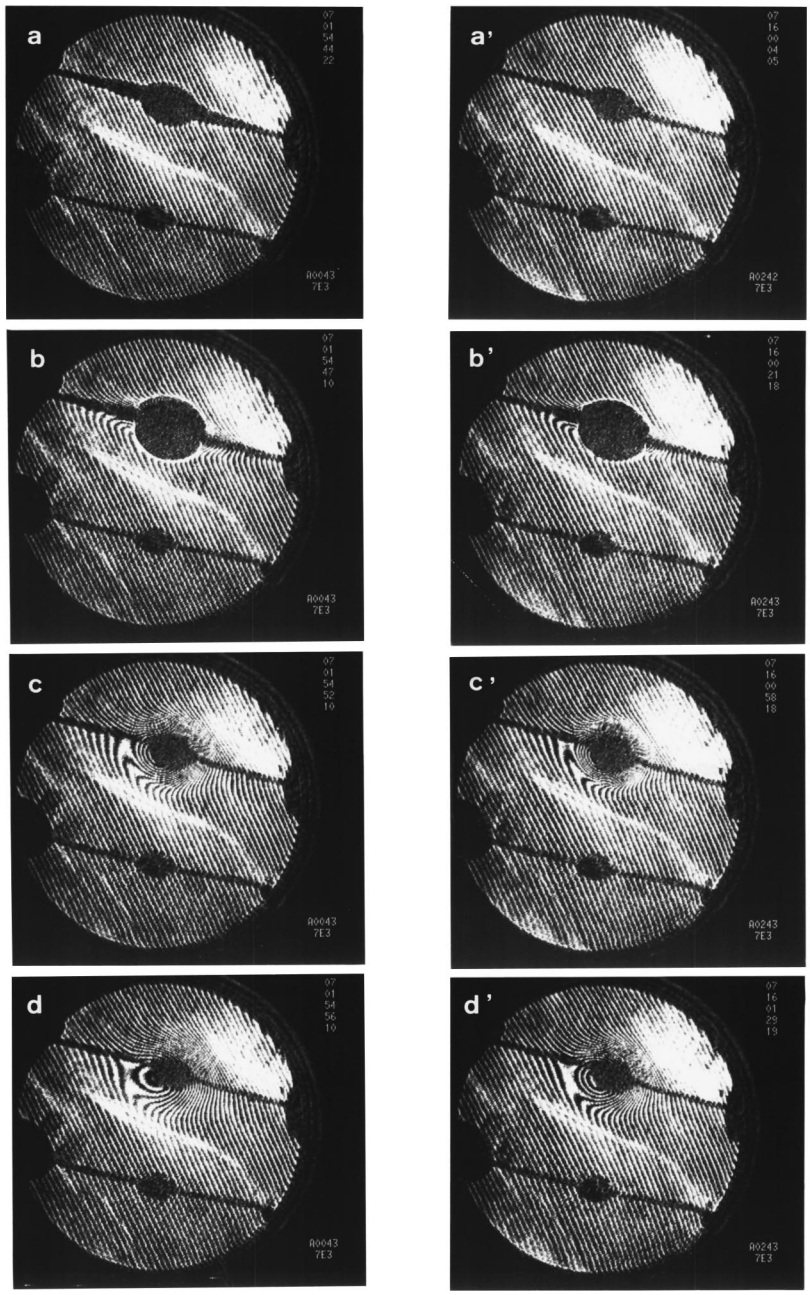

FIG. 7. Time sequence of the density inhomogeneity relaxation after a 480 ms heat pulse (microgravity conditions). Notice the hot boundary layer [TH1 HBL in Fig. 4(c)], which forms around the upper heating thermistor (the black region increase around TH1). Also notice the fading out of this boundary layer and the reappearance of distorted fringes as time proceeds. Left: Initial fluid temperature $T_i = T_c + 16.8$ K: (a) 480 ms after the beginning of the heat pulse; (b) 3 s; (c) 8 s; and (d) 12 s; right: initial fluid temperature $T_i = T_c + 800$ mK: (a′) 480 ms after the beginning of the heat pulse, (b′) 18 s, (c′) 55 s, and (d′) 86 s. Time comparison of the relaxation process of the HBL density inhomogeneities for the two different initial temperatures T_i evidences the diffusive critical slowing down.

12(a)]. This fast heating period is due to the development of the HBL during Δt_H (estimated in Appendix B to be ≈ 2.5 s). The bulk fluid is heated uniformly as shown by the shift of the whole fringe pattern, the fringes remaining straight.

Cooling towards the thermostat temperature proceeds more slowly [see Fig. 12(b)]. For the sake of comparison, we also report in Fig. 12(c) the HBL temperature as measured by TH1, $T_{\mathrm{HW}} = T_{\mathrm{TH1}}$ (log-log plot). Although the HBL is always hotter than the bulk, it does not apparently interfere with the bulk uniform cooling ensured by the CBL.

Similar results are obtained at $T_c + 15.9$ K and $T_c + 0.8$ K but at this last temperature the bulk variation is significantly smaller, making the analysis difficult. When $T_i < T_c + 0.8$ K, *no temperature rise can be detected* by the TH2 thermistor. Such a lowering of the temperature change

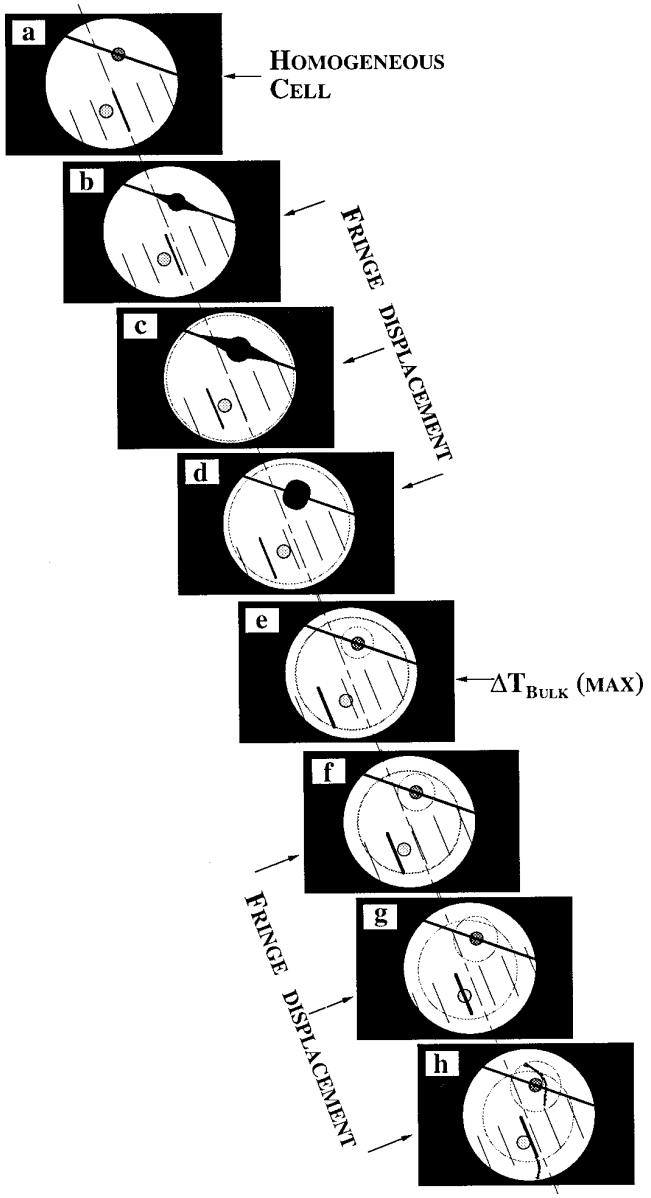

FIG. 8. Schematic representation of the temporal sequence of a pulse heating and of the subsequent thermal relaxation (microgravity). This sequence illustrates the main features of the observed phenomenon during the real time sequence of Fig. 7 (see the text).

in the bulk is due to the divergence of C_v and to the increasing efficiency of the CBL: the fluids acts as a true thermal short circuit, as predicted in [13].

V. QUANTITATIVE COMPARISON WITH THE 1D MODEL

A. The bulk temperature behavior at $T_c+16.8$ K

1. Characteristic length of the model

As discussed in Sec. II, knowledge of L (the characteristic length) and $P(t)$ (the heating power evolution) is mandatory for a comparison with experiments.

The smallest length scale $L=1.5$ mm [Eq. (14)] corresponds to a characteristic time t_c (≈ 3.5 s) similar to our estimation of Δt_H (≈ 2.5 s). Furthermore, t_c is larger than

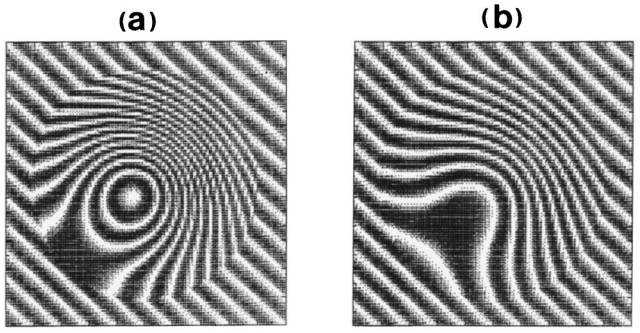

FIG. 9. Numerical simulation of the interference fringe pattern. Effect of a 2D Gaussian distributed refractive index inhomogeneity in a uniform refractive index medium (see [2]). (a) Value of the central maximum amplitude $\delta n/n=10^{-4}$, (b) value $\delta n/n=0.5\times10^{-4}$. Notice the striking similarity of the fringe distorsion with the interferometric pattern observed on Figs. 7(d) and 7(d′) within the hot boundary layer [TH1HBL in Fig. 4(c)].

the typical equilibration response time of the thermostat (≈ 1 s, see Table II), which validates the boundary condition of a perfectly thermostated wall $[T(x=L)=T_i]$ as used in the model.

The simulation at $T_c+16.8$ K as detailed in Appendix B gives access to the total energy ($Q=8.1$ mJ) sent in the fluid by the heating thermistor. From Q, an estimated time profile for the heat flux $P(t)$ is proposed, under the form of a rapid rise to a maximum value during 0.6 s (corresponding to the electrical supplying period added to the time response of the thermistor), followed by a slower decrease (corresponding to the heat losses period by leads). The value of the maximum and the slope of the decrease are fixed by two criteria: the total energy provided, and the fact that the maximum of the resulting bulk temperature must be located around 3 s after the beginning of the heating.

The analytical results based on this heat flux are compared in the following to the bulk temperature relaxation at

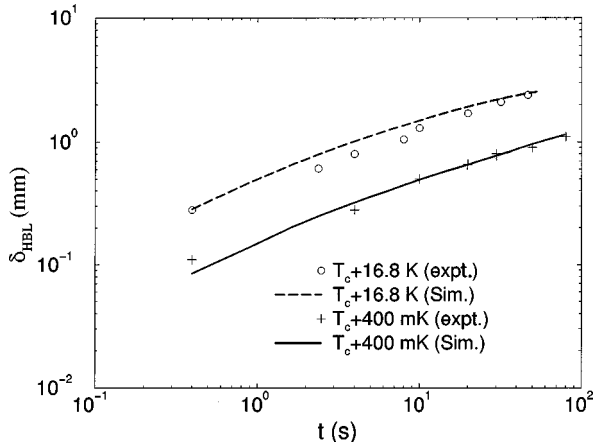

FIG. 10. Experimental thickness δ_{HBL} (Expt.) of the hot boundary layer [TH1HBL in Fig. 4(c)] vs time during heating and cooling periods at two different equilibrium temperatures. Open circles: $T_i=T_c+16.8$ K; crosses: $T_i=T_c+400$ mK. Measurements are performed after the end of the electrical excitation period (480 ms) of the TH1 thermistor. The numerical simulation (Sim.) is based on a purely diffusive process (see [27]). Dashed line: $T_i=T_c+16.8$ K; solid line: $T_i=T_c+400$ mK.

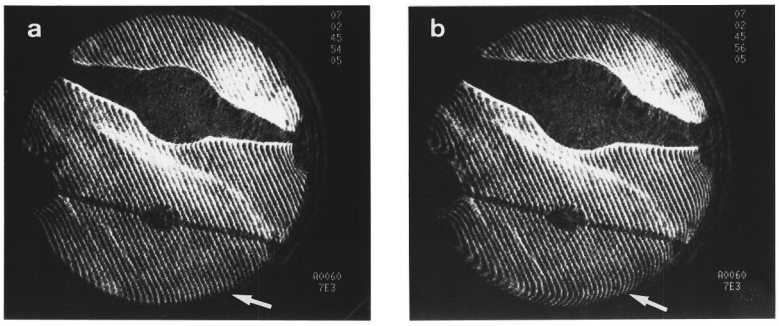

FIG. 11. Cold boundary layer formation during a continuous heat pulse [see the CBL region defined on the Fig. 4(c)]. (a) $t=4$ s after the beginning of the pulse, (b) $t=6$ s. The arrows note the fringe deformations close to the cell wall (thermostated at the initial equilibrium temperature $T_i=T_c+16.8$ K), while the bulk fringes remain straight. Due to the continuous heating at the TH1 level and to the correlated continuous increase of the bulk temperature, this CBL appearance corresponds to a significant increase of the local density, here well marked by a significant left bending of the fringes [see also Fig. 4(c)].

$T_c+16.8$ K (corrected at $t<60$ s of 3 mK due to the thermistor self-heating). From this analysis, first we will check our estimation of L and, second, we will define the time evolution of the heat flux sent in the fluid.

2. Fits of the bulk temperature relaxation

After the end of the heat pulse, the bulk temperature progressively tends to behave like the impulse response $F(t)$, whatever the time profile of the flux [13]. The data corresponding to a time long enough after the end of the heating can be fitted to Eq. (3), or more explicitly to

$$\Delta T_b = A_0 \exp\left(\frac{t}{t_c}\right) \mathrm{erfc}\left(\frac{t}{t_c}\right)^{1/2}, \tag{20}$$

where ΔT_b is the bulk temperature rise as measured by TH2. t_c and $A_0=(Q/m)/c_v$ are adjustable parameters (Q is the total energy sent at the hot wall). Fits have been performed in two different ranges, 5–60 s or 10–60 s. If 5 s is a sufficient time delay, the result of the fit should be the same in both cases, the fluid having ''forgotten'' the time history of the heat flux. The range is limited to 60 s because this time is the upper limit of the high rate measurements.

The result of these fits is summarized in Table III. The amplitudes A_0 and t_c show a large discrepancy between the ranges. This is due to the fact that for large enough values of t, ΔT_b tends to behave like $A_0\sqrt{t_c/t}$. Consequently, it becomes more and more difficult for a fitting algorithm to discriminate between the relative influence of A_0 and t_c, even if the global fit is correct. This point is confirmed by the calculation of the product $A_0\sqrt{t_c}$ for each fit, which leads to similar results in both cases (the difference is less than 3%). In order to obtain more accuracy in the value of t_c, we now consider the estimate of the total energy sent into the fluid ($Q=8.1$ mJ) and impose $A_0=(Q/m)/c_v=22.6$ mK. The results of the fits with t_c as the only free parameter gives only one value, $t_c\approx 4.3$ s (Table III). This value compares well with the value inferred from Eq. (14) ($t_c=3.5$ s with $L=1.5$ mm) and shows the relevance of the ratio fluid volume to cold wall area for adapting the 1D model to the experiment.

Let us comment on the thermistor self-heating in the high-rate measurement mode. In order to estimate the temperature bias, some fits were made on the experimental data, based on the function $A_1/\sqrt{t}$ where A_1 is a free parameter. A_1 was calculated on experimental data ranging from 5 to 300 s, with different self-heating corrections applied between 5 and 60 s. The best fit corresponds to the expected value of 3 mK, which independently confirms the manufacturer's specifications.

We consider now the value $L=1.5$ mm as set in the model prediction and return to $P(t)$. The data which are concerned correspond mainly to the temperature rise at early times [Fig. 12(a)]. According to Fig. 15, the two parameters are Δt_H and the maximum power (at $t=0.6$ s) with the 8.1 mJ value as a constraint for the integrated total energy Q. The best fit is shown in Fig. 12(a). It corresponds to a value $\Delta t_H=3.8$ s, comparable to but slightly larger than our previous estimation (2.5 s).

B. The HBL relaxation at TH1

1. Critical behavior of the HBL temperature

The following approach is based on Eq. (6), where we have focused our attention on the time dependence of $T_{\mathrm{HW}}(x=0)$ for the intermediate range $\Delta t_H<t<t_D$. For temperatures nearer to T_c than 1 K, $t_c<\Delta t_H$. Using Eq. (6), we have determined that the late-time response of $\Delta T_{\mathrm{HW}}=T_{\mathrm{HW}}-T_i$ tends to behave according to the following law:

$$\Delta T_{\mathrm{HW}}(x=0)=A\sqrt{t}. \tag{21}$$

The amplitude A is proportional to the total energy sent to the fluid but does not depend on the time history of the heat flux. For the same total energy sent into the fluid at each temperature T_i, Eq. (6) leads to

$$A\propto(\sqrt{t_c})/Cv, \tag{22}$$

which asymptotically vanishes as $(T_i-T_c)^{0.91}$ (see Appendix A).

If the experimental data measured by TH1 are considered starting from a sufficiently long time (>6 s) after the end of the heating pulse, the $t^{-1/2}$ law is observed. As a consequence, we have chosen to perform the comparison between the experimental results and model results for $t=10$ s after the heating pulse beginning. The measured values have been

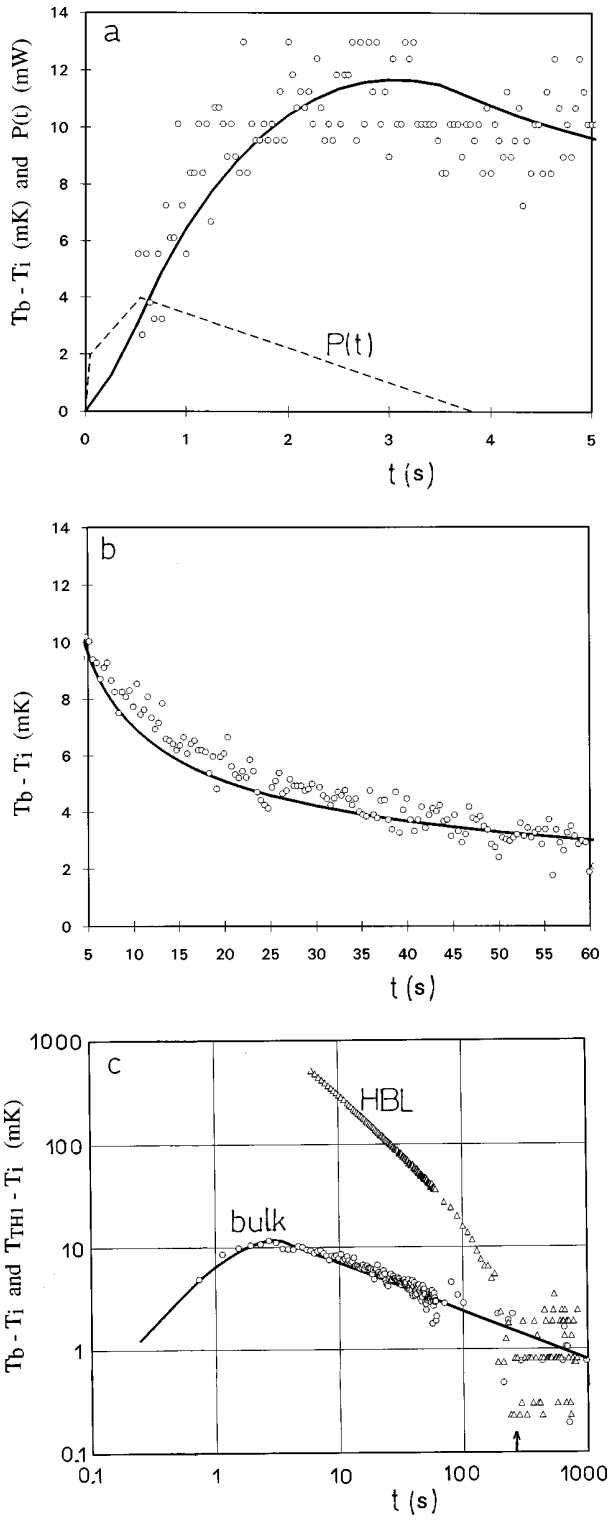

FIG. 12. Temperature relaxation $(T_b - T_i)$ of the bulk fluid vs time as measured by the TH2 thermistor (open circles) and as fitted by our present model (solid lines). Initial equilibrium fluid temperature $T_i = T_c + 16.8$ K. (a) Linear plot during the first 5 s after the beginning of the heat pulse; time power profile $P(t)$ of the heat pulse is given by the broken line (see Appendix B); (b) linear plot during the period 5–60 s; (c) log-log plot for the whole time range; the temperature relaxation of the hot boundary layer measured by the TH1 thermistor is also reported (opened triangles). The arrow marks the typical time to restore complete density and temperature equilibration.

TABLE III. Fitting results of the bulk temperature relaxation ΔT_b measured by TH2 using Eq. (20) where A_0 and t_c are the adjustable parameters. The values in parentheses have been imposed in the fit (see text).

Time interval of the fit (s)	A_0 (mK)	t_c (s)
5–60	38.8	1.3
	(22.6)	4.36
10–60	149	0.085
	(22.6)	4.26

normalized to the same value of the total energy (1 mJ) using the calculated power delivered by the thermistor from the Joule effect (see Appendix B). Moreover, to adapt the 3D experiment to the model conditions, the temperature differences $T_{TH1} - T_i$ have been also divided by the area ratio from the cold wall to the hot wall ($S_{CW}/S_{HW} \cong 80$, see Sec. II C). The comparison between these normalized experimental values ΔT^n_{TH1} ($x = 0$, $t = 10$ s, $Q = 1$ mJ, $S = S_{CW}$), and the corresponding calculated values from the model is made in Fig. 13. Quantitative agreement is noticeable in regard to the uncertainties attached to each estimation of these above quantities. This is an experimental observation directly related to the expected critical shortening of the PE characteristic time. Moreover, the exponent 0.91 associated with A assumes that the critical exponent associated with D_T has its asymptotic value of 0.67. This assumption is in default for the temperature range of our measurements. Although the temperature dependence of D_T is complicated to analyze in this temperature range, it can be approximated by an effective exponent value of 0.8 for most of pure fluids [28]. Then the effective exponent of the temperature dependence of A can be lowered to a value of 0.8, which is closer to the apparent experimental slope in Fig. 13.

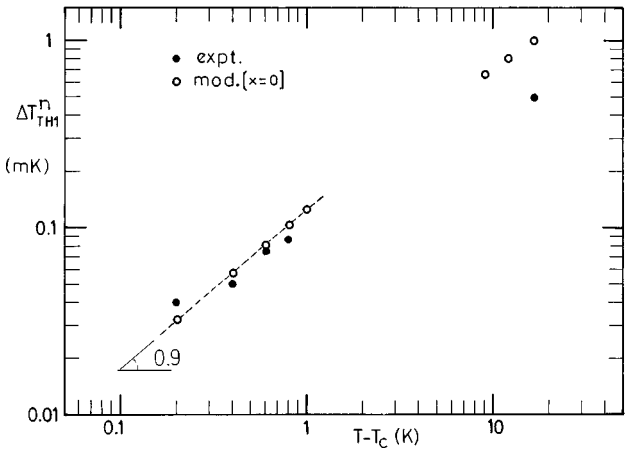

FIG. 13. Normalized hot wall temperature ΔT^n_{TH1} ($x = 0$, $t = 10$ s, $Q = 1$ mJ) as a function of $(T - T_c)$ [see text and Eq. (21)]. Filled circles: experiment from the TH1 measurements (see text); opened circles: 1D computation from the model. Notice that the normalized HBL experimental temperature is related to the amplitude A of Eq. (21) and decreases as $(t_c)^{1/2}/Cv$ as T approaches T_c [see Eq. (22)], in agreement with the predicted critical asymptotic behavior of t_c [see Eqs. (5) and (2)] and Cv (see text).

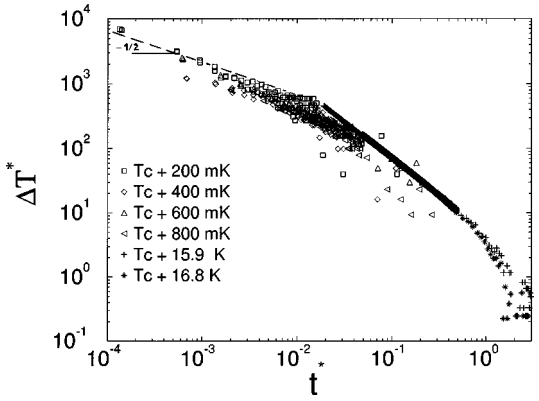

FIG. 14. Log-log plot of $\Delta T^* = mc_p[T_{\mathrm{HW}}(t) - T_i]/Q$ vs the reduced time $t^* = t/t_D$. Near T_c, theory predicts an initial slope of $-1/2$ [see the text and Eqs. (6) and (7)]. $T_{\mathrm{HW}}(t)$ is the relaxation temperature of the hot boundary layer [TH1 HBL in Fig. 4(c)] measured by the TH1 thermistor.

2. Diffusive scaling of the HBL temperature relaxation

The form of the right member of the Eq. (6) suggests a normalized scaling for the relaxation of the hot wall temperature. Figure 14 shows a log-log plot of the relaxation of the reduced HW temperature $\Delta T^* = mc_p[T_{\mathrm{HW}}(t) - T_i]/Q$ versus the reduced time $t^* = t/t_D$ for the different equilibrium temperatures. Here, m is the mass of the whole fluid. All data collapse to a single curve with an initial power-law behavior $(t^*)^{-1/2}$. Such a power law is found for diffusive processes taking place in semi-infinite media; for small values of t^*, the HBL relaxation is not influenced by the finite dimensions of the cell. We notice that when $t^* \cong 1$, $\Delta T^* \cong 1$. This indicates that, for $t \cong t_D$, the energy initially transmitted into the HBL has diffused into the bulk. This confirms again the diffusive character of the HBL relaxation.

VI. GENERAL CONCLUSIONS

The dynamics of the piston effect after a heat pulse (heating and subsequent cooling) in the fluid is ruled both by the diffusion time t_D and by the PE time t_c. Three distinctive regions are directly observed in the sample. The first region is a hot boundary layer, centered on the heat source, which shows large coupled density-temperature inhomogeneities. This part is cooled mainly by a diffusive process whose temperature relaxation is slowed down near the critical point. The second region is the bulk fluid, which is uniform in temperature and density. The presence of thermostated walls induces a weak cold boundary layer (the third region), which cools the bulk by the PE mechanism. Then, complete equilibration in temperature and density of the fluid is governed by the diffusion time t_D, which corresponds to the slowest transport mechanism.

A proper design of an experimental cell has thus given access simultaneously to a direct observation of the whole fluid sample and to precise quantitative measurements, on the different time scales of the process. In particular, it was necessary to obtain a good separation between the main characteristic times of the experimental device $(t_{R,\mathrm{cell}}, \Delta t_{\mathrm{elec}}, \Delta t_H)$ and of the fluid sample (t_c, t_D). This first point was achieved by a proper choice of the cell materials, and by the use of a small heating device immersed in the fluid instead of a global cell heating. On the other hand, having a high area ratio between the inner heating thermistor and the outer isothermal cell wall proved to be a good choice. Indeed, a large cold surface results in a relatively fast bulk temperature relaxation, even far from T_c. The observation is thus made easier, in particular for the shift of the interferometric pattern. At the same time, a small heating surface, for the same heating power, results in a higher boundary layer temperature, which is convenient to make measurements near T_c. Here the bulk fluid becomes a thermal short circuit with no measurement available for the bulk temperature modification due to the t_c shortening and to the C_V increasing.

Note added in proof. A recently published paper [29] analyzed the density changes associated with the late stage of thermal equilibration near the critical point of SF_6. The conclusion of Wilkinson *et al.* is in agreement with those presented here for the heat diffusion decaying mode in an isothermal container.

ACKNOWLEDGMENTS

This work was supported by CNES. We gratefully acknowledge the ALICE team and especially P. Koutsikidès and J.-M. Laherrère for their support. We thank all individuals involved in the French-Russian missions on MIR station (ANTARES, 1992, and ALTAIR, 1993). We feel indebted in particular to the crews of both missions, with special mention to the French cosmonauts M. Tognini and J. P. Haigneré.

APPENDIX A: DETAILS ON THE THEORETICAL MODEL

As mentioned in the core of the text, the theoretical model proposed here is an extension to real fluids of the van der Waals model developed in [13]. As a consequence, only the information necessary to understand this extension will be given here. The detailed procedure and calculation can be drawn from the analogy with the referenced paper.

A one-dimensional container is filled with a near-critical fluid on the critical isochore, in the one-phase region. The fluid, initially at thermal and mechanical equilibrium, is submitted to a heat flux $P(t)$ on the left wall of the container $(x=0)$, while the right wall $(x=L)$ is thermostated at the initial temperature.

The model is based on the 1D unsteady compressible Navier-Stokes equations written for a Newtonian fluid. In what follows, the subscript i refers to the initial conditions and PG to the perfect gas. An asterisk is used to indicate a dimensionless variable.

The equations are made dimensionless by using the following parameters (respectively denoting density, temperature, pressure, sound velocity, time, and space variables):

$$\rho^* = \frac{\rho}{\rho_c}, \quad T^* = \frac{T}{T_c}, \quad p^* = \frac{p}{\rho_c r T_c}, \quad u^* = \frac{u}{\sqrt{\gamma_{0\mathrm{PG}} r T_c}},$$

$$t^* = \frac{t\sqrt{\gamma_{0\mathrm{PG}} r T_c}}{L}\left(\frac{Cv_{\mathrm{PG}}}{Cv}\right)^{1/2}, \quad x^* = \frac{x}{L}, \qquad \text{(A1)}$$

where r is the specific gas constant (in J kg^{-1} K^{-1}).

The introduction of $\sqrt{Cv}$ in the expression of the time variable t^* enables the vanishing sound velocity to be taken into account in the vicinity of the CP. In the same way as in [13], a small parameter ε^* appears in the energy equations, in front of the heat diffusion term. ε^* is defined by

$$\varepsilon^* = \mathrm{Pr}_{\mathrm{PG}} \frac{t_{a\mathrm{PG}}}{t_{\mathrm{DPG}}} \ll 1, \tag{A2}$$

with

$$t_{\mathrm{aPG}} = \frac{L}{\sqrt{\gamma_{0\mathrm{PG}} r T_c}} \quad \text{(typical acoustic time for the PG)} \tag{A3}$$

and

$$t_{\mathrm{DPG}} = \frac{L^2 \rho_c C p_{\mathrm{PG}}}{\lambda_{\mathrm{PG}}} \quad \text{(typical diffusion time for the PG)}. \tag{A4}$$

Instead of a van der Waals equation of state, a linearized nondimensional equation of state is used here, written in the most general case:

$$p^* - p_i^* = (T^* - T_i^*)\left(\frac{\partial p^*}{\partial T^*}\right)_{\rho^*} + (\rho^* - \rho_i^*)\left(\frac{\partial p^*}{\partial \rho^*}\right)_{T^*}, \tag{A5}$$

where the pressure p_i^* and the partial derivatives are taken at (T_i^*, ρ_i^*).

The initial and boundary conditions set on these equations are

$$T^*(t^*=0,x^*) = T_i^* = 1 + \Delta T^*,$$

$$p^*(t^*=0,x^*) = p_i^*(1+\Delta T^*,1) = p_{i\,\mathrm{expt}}^*,$$

$$\rho^*(t^*=0,x^*) = \rho_i^* = 1,$$

$$u^*(t^*=0,x^*) = 0,$$

$$-\frac{\lambda}{\lambda_{\mathrm{PG}}} T_x^*(t^*,x^*=0) = \varphi^* \frac{P(t^*)}{P_{\max}},$$

$$\varphi^* = \frac{P_{\max} L}{S \lambda_{\mathrm{PG}} T_c},$$

$$T^*(t^*,x^*=1) = T_i^* = 1 + \Delta T^*, \tag{A6}$$

where $p_{i\,\mathrm{expt}}^*$ is obtained from the experimental pressure at each considered equilibrium temperature along the critical isochore (see Table I). $P_{\max}/S$ is the maximum value reached by the heat flux per unit area during its time evolution (S is the surface area of the heated wall). φ^* is usually very small ($\varphi^* \ll 1$).

The fact that the initial conditions are chosen near the CP leads to $\Delta T^* \ll 1$.

Using dimensionless equations allows then a clear analysis of the relative orders of magnitude of the different contributions. This is done by considering ε^* and ΔT^* as infinitesimally small quantities, and solving the equations under the form of matched asymptotic expansions based on the limits $\varepsilon^* \to 0$ and $\Delta T^* \to 0$. The presence of ε^* in front of the diffusive term in the equation of energy leads to the introduction of two boundary layers near the extremities of the container. Three coupled linearized systems of equations are thus obtained, for the HBL, the bulk, and the CBL. When solved on the acoustic time scale, these systems lead to the response briefly described in introduction: (i) When the heat flux is imposed on the wall, heat diffuses in a thin boundary layer which expands strongly due to the high compressibility (HBL). (ii) This expansion drives a compression wave in the bulk, that propagates back and forth as it reflects on the boundaries. (iii) During its repeated travels, the compression wave slowly raises the bulk temperature in a quasihomogeneous way.

After a certain time, the bulk temperature increases to a point where it becomes of the same order as the HBL temperature, thus defining the PE time scale. To take this time scale into account in the calculation, a new time variable is introduced into the system, defined as

$$\tau^* = \varepsilon^* \frac{\lambda}{\lambda_{\mathrm{PG}}} \left(\frac{Cv_{\mathrm{PG}}}{Cv}\right)^{3/2} \left(\frac{\partial \rho^*}{\partial \rho^*}\right)_{T^*} t^*. \tag{A7}$$

This scale has been found by calculating, on the basis of the acoustic solutions, the necessary time for the bulk temperature to become of the same order as the HBL temperature. Here, the critical speeding up is expressed by the fact that t^*/τ^* goes to zero like $(\Delta T^*)^{1.6}$. The system is now rewritten in terms of ρ^*, T^*, p^*, u^*, x^*, and τ^*. The same matched asymptotic expansions procedure as above is used again, to obtain the PE time-scale solutions. The following points are found: (i) Near the heated wall, the fluid in the HBL expands, and thus compresses the bulk fluid (homogeneous heating). (ii) Near the thermostated wall, another layer forms where the fluid is cooled (CBL). This cooling provokes a contraction of the fluid, and thus an expansion of the bulk (homogeneous cooling). (iii) The bulk response is the result of the competition between these two opposite effects.

Thanks to the global Navier-Stokes approach, it is possible through these calculations to access the time and space variations of any thermophysical parameter of this problem. In particular, the bulk temperature, the temperature at the heated wall, and the velocity at the edge of the HBL are given in the core of the paper. The corresponding calculation can easily be deduced from Ref. [13] and the above information.

APPENDIX B: MODELING THE HEAT PULSE

We have performed a numerical simulation of an ideal conduction problem assuming a finite spherical geometry for the thermistor unit. Here we report only the main results. The central part of TH1 is assimilated to a heat source sphere ($S1$) of 0.2 mm diameter where electrical power is delivered at constant voltage U. The electric power is calculated from the characteristics given by THERMOMETRICS for the B35 thermobeads. The glass coating of the thermistor is accounted for by considering a second sphere ($S2$) of 0.9 mm

outer diameter enclosing $S1$. Both $S1$ and $S2$ are considered to be made of identical glass material having the same thermal properties as commercial zirconia (Table II). This material modeling is close to the real thermistor as shown by the calculated thermal time constants: 63% of the maximum temperature rise occurs in 79 ms (Table II), a value close to the 100 ms value given by the manufacturer. Moreover, the temperature increase due to the dissipated power on the glass material during the high rate temperature measurements is 3 mK, a value that agrees with the technical data provided by the supplier and the observations in Secs. IV and V.

In the simulation, $S1+S2$ are located at the center of an infinite fluid medium with spherical symmetry. The fluid is homogeneous in density ($\rho=\rho_c$) and its characteristics are those along the critical isochore. Time discretization for numerical calculations is 25 ms. The effect of the thermistor leads is not considered in this model.

It appears that the distance to the critical point is a key parameter to describe the thermistor behavior. When the fluid is initially at $T_c+16.8$ K, the temperature change at the center of $S1$ follows (t in s, T in K):

$$\Delta T(t)\approx T_i+18.5t^{1/2}. \tag{B1}$$

This temperature rise causes the thermistor resistance to change accordingly. After $t=480$ ms, the total energy developed in the core of the thermistor can be estimated to $Q_{\rm elec}\approx 14.4$ mJ (whose 37% is due to the self-heating of the thermistor) and the external surface temperature change on $S2$ is close to 5 K. When using the thermal data of Table I, the energy needed to obtain a mean temperature increase of 5 K is 6.3 mJ, which represents 46% of $Q_{\rm elec}$. This result shows that a little more than half of the total energy can be dissipated into the HBL surrounding the thermistor.

When the fluid is closer to the critical point (range $[T_c+0.1\ {\rm K}-T_c+1\ {\rm K}]$), the temperature change in the center of $S1$ follows (t in s, T in K):

$$\Delta T(t)\approx T_i+12t^{1/2}. \tag{B2}$$

The energy is estimated to be $Q_{\rm elec}\approx 7.4$ mJ after a 480 ms pulse (26% is due to self-heating) and the corresponding mean temperature change of $S1+S2$ is close to 2 K. The energy stored in the thermistor is of the order of 3 mJ, i.e., the same percentage as at higher temperature although the total energy has been divided by approximately two (due to the ratio value $R_{\rm TH1}(48\ ^\circ{\rm C})/R_{\rm TH1}(32\ ^\circ{\rm C})\cong 1/2$).

Let us note the small value of the total energy sent by the heat pulse, which makes the SCU temperature practically unchanged (the temperature rise should be lower than 15 μK at $T_i=T_c+16.8$ K if the total energy of 14.4 mJ were injected instantaneously in the SCU). The external boundary conditions of the fluid are then isothermal during temperature relaxation.

The above model suffers from two defects. (i) It neglects the heat losses through the lead wires. (ii) It considers only heat transfer into the HBL and neglects the energy that is transferred into the bulk by the PE mechanism. This last contribution remains small, due to the low yield of the PE (see Sec. II D). In contrast, the self-heating of the thermistor

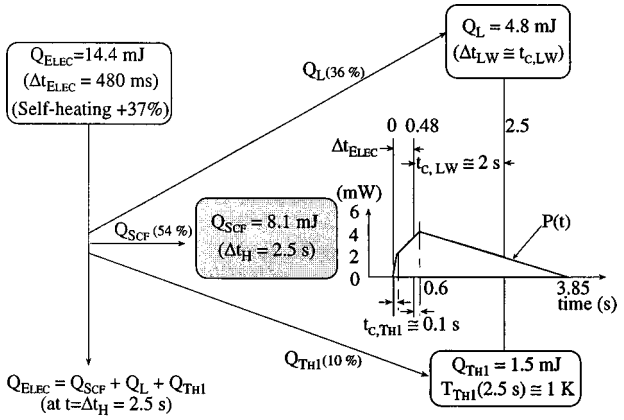

FIG. 15. Partition of the energy (in the absence of convection) delivered by the Joule effect during a 480 ms electrical supplying of the heating thermistor TH1 (see text and Appendix B). The fluid equilibrium temperature is $T=T_c+16.8$ K. $P(t)$ is the schematic time profile of the heat flux delivered into the critical fluid from the external surface of the heating TH1 thermistor.

increases the heat losses through the lead wires. Although a precise evaluation is difficult to make, an order of magnitude can be estimated for the energy lost during the thermal time response of the lead wire, i.e., 2 s. We consider the fluid at $T_c+16.8$ K. We assume a linear temperature evolution from 5 K, the above estimated temperature at the end of the electrical pulse, to 1 K, an arbitrary choice (the corresponding energy uncertainty is 0.5 mJ); we assume also the temperature inhomogeneity along the wire axis to be linear with a spatial extension of 1 mm. We obtain then a value of 7 mJ. From the above analysis, it appears that the energy part (6.3 mJ) used to heat the external surface of the thermistor is comparable to the energy part lost through the lead wires.

A schematic representation of the heat pulse partition is given in Fig. 15. The total heat energy $Q_{\rm elec}$ ($=14.4$ mJ) produced during the $\Delta t_{\rm elec}$ ($=480$ ms) period is separated into two main contributions $Q_{\rm TH1}+Q_L$ ($=4.8+1.5$ mJ) and $Q_{\rm SCF}$ ($=8.1$ mJ) at the estimated end of the heat pulse duration Δt_H ($\Delta t_H\approx\Delta t_{\rm elec}+t_{C,\rm LW}\approx 2.5$ s, see below). $Q_{\rm TH1}$ corresponds to the heat necessary to give the temperature elevation ($+1$ K) of the thermistor unit. Q_L is the energy part directly lost by solid conduction through the lead wires. $Q_{\rm SCF}$ is then the *true* total energy sent into the HBL and in the bulk. We can estimate that, at least during the typical response time ($t_{C,\rm LW}$) of the lead wires and of the SCU ($t_{C,\rm SCU}$), i.e., approximatively 2 s, TH1 can still heat the fluid. This is why the heat pulse duration $\Delta t_H\approx\Delta t_{\rm elec}+t_{C,\rm LW}\approx 2.5$ s lasts longer than the electric supplied pulse. As a consequence, we obtain 3.24 mW as a mean value for the power energy. However, a schematic more realistic time profile of the power energy $P(t)$ is also reported on the Fig. 15. It corresponds to properly considering the part of the thermistor time constant $t_{C,\rm TH1}$ (≈ 100 ms) and the predominant initial heating due to the thermistor self-heating mode during the supplied period $\Delta t_{\rm elec}$ (see the main text for the correct evaluation of $P(t)$ from the results obtained in microgravity).

[1] M. Bonetti, F. Perrot, D. Beysens, and Y. Garrabos, Phys. Rev. E **49**, 4779 (1994).
[2] M. Bonetti, F. Perrot, D. Beysens, and Y. Garrabos, in Proceedings of the 12th Symposium on Thermophysical Properties, Boulder, Colorado, 1994, edited by J. M. H. Levelt-Sengers and A. Cezairliyan [Int. J. Thermophys. **16**, 1059 (1995)].
[3] Experiments were performed on the instrument ALICE (Analyse des Liquides Critiques dans l'Espace) which was developed by CNES for the analysis of fluids close to the critical point in microgravity.
[4] J. M. Laherrère and P. Koutsikidès, Acta Astron. **29**, 861 (1993).
[5] A. M. Radhwan and D. R. Kassoy, J. Eng. Math. **18**, 183 (1984).
[6] A. Onuki, H. Hao, and R. A. Ferrell, Phys. Rev. A **41**, 2256 (1990).
[7] H. Boukari, J. N. Shaumeyer, M. E. Briggs, and R. W. Gammon, Phys. Rev. A **41**, 2260 (1990).
[8] B. Zappoli, D. Bailly, Y. Garrabos, B. Le Neindre, P. Guénoun, and D. Beysens, Phys. Rev. A **41**, 2264 (1990).
[9] A. Onuki and R. A. Ferrell, Physica A **164**, 245 (1990).
[10] B. Zappoli, Phys. Fluids A **4**, 1040 (1992).
[11] R. A. Ferrell and H. Hao, Physica A **197**, 23 (1993).
[12] B. Zappoli and A. Durand-Daubin, Phys. Fluids **6**, 1929 (1994).
[13] B. Zappoli and P. Carlès, Eur. J. Mech. B **14**, 41 (1995).
[14] K. Nitsche and J. Straub, Naturwissenschaften **73**, 370 (1986).
[15] H. Klein, G. Schmitz, and D. Woerman, Phys. Rev. A **43**, 4562 (1991).
[16] P. Guénoun, B. Khalil, D. Beysens, Y. Garrabos, F. Kammoun, B. Le Neindre, and B. Zappoli, Phys. Rev. E **47**, 1531 (1993).
[17] Y. Garrabos, B. Le Neindre, P. Guénoun, F. Perrot, and D. Beysens, Microgravity Sci. Technol. **2**, 108 (1993).
[18] H. Boukari, M. E. Briggs, J. N. Shaumeyer, and R. W. Gammon, Phys. Rev. Lett. **65**, 2654 (1990).
[19] R. P. Behringer, A. Onuki, and H. Meyer, J. Low Temp. Phys. **81**, 71 (1990).
[20] F. Zhong and H. Meyer, in *Fluid Mechanics Phenomena in Microgravity*, edited by D. A. Siginer, R. L. Thompson, and L. M. Trefethen, special issue of J. Am. Soc. Mech. Eng. **174**, 139 (1993).
[21] F. Zhong and H. Meyer, Phys. Rev. E **51**, 3223 (1995).
[22] J. Straub, L. Eicher, and A. Haupt, Phys. Rev. E **51**, 5556 (1995).
[23] P. Carlès, thesis, INP Toulouse, France (1995).
[24] J. V. Sengers, in *Critical Phenomena*, Proceedings of the International School of Physics ''Enrico Fermi,'' Course LI, edited by M. S Green (Academic, New York, 1971), p. 445.
[25] H. Klein and B. Feuerbacher, Phys. Lett. A **123**, 183 (1987).
[26] H. S. Carslaw and J. C. Jaeger, *Conduction of Heat in Solids*, 2nd ed. (Oxford University Press, London, 1959).
[27] T. Fröhlich, S. Bouquet, M. Bonetti, Y. Garrabos, and D. Beysens, Physica A **218**, 419 (1995).
[28] J. Luettmer-Strathmann, J. V. Sengers, and G. A. Olchowy, J. Chem. Phys. **103**, 7482 (1995), and references therein.
[29] R. A. Wilkinson, G. A. Zimmerli, H. Hao, M. R. Moldover, R. F. Berg, W. L. Johnson, R. A. Ferrell, and R. W. Gammon, Phys. Rev. E **57**, 436 (1998).